Blind Compressed Sensing-based Ultrafast Chemical Exchange Saturation Transfer (CEST) Imaging

Hye-Young Heo[1,2], Sampada Bhave[3], Mathews Jacob[3], and Jinyuan Zhou[1,2]

[1]The Russell H. Morgan Department of Radiology and Radiological Science, Johns Hopkins University School of Medicine, Baltimore, MD, United States, [2]F.M. Kirby Research Center for Functional Brain Imaging, Kennedy Krieger Institute, Baltimore, MD, United States, [3]Department of Electrical and Computer Engineering, University of Iowa, Iowa City, IA, United States

Synopsis

CEST imaging, such as amide proton transfer (APT) imaging, is a novel, clinically valuable molecular MRI technique that can give contrast due to a change in water signal caused by chemical exchange with saturated solute protons. However, its clinical translation is still limited by its relatively long scan time because a series of RF saturation frequencies are unavoidably acquired. Here, we present a highly accelerated CEST imaging technique (up to 10-fold) using a novel blind compressed sensing framework.

Introduction

Chemical exchange saturation transfer (CEST) imaging is a promising molecular MRI technique in which the contrast is caused by a change in water signal intensity due to chemical exchange with saturated solute protons (1). CEST imaging can detect many low-concentration biomolecules in tissue, such as proteins with amide proton transfer (APT) imaging (2), glycosaminoglycan using GagCEST (3), and glutamate using GluCEST (4), and has much potential in the clinic, such as detecting cancer (5-7), stroke (8,9), and Parkinson's disease (10). However, CEST MRI typically requires relatively long scan times, due to the use of multiple RF saturation frequencies, possible multiple acquisitions to increase SNRs, and a long RF saturation pulse (or multi-pulse train), thus limiting its clinical translation. Herein, as proof of principle, we demonstrated the feasibility of an ultrafast APT imaging (up to 10-fold) based on blind compressed sensing (BCS), which models the dynamic CEST signal as a weighted linear combination of temporal basis functions from a dictionary learned from the undersampled measurements (Fig. 1).

Methods

Dynamic CEST signal recovery, $\gamma(x, w)=\sum U^*(x)V^*(w)$ was formulated as a constrained optimization problem (11):

$$[U^*, V^*] = argmin[\|A(UV - b)\|_F^2 + \lambda_1\|U\|_1], s.t. \|V\|_F^2 < 1$$

where the criterion is a linear combination of data consistency term (*b*=undersampled data, *A*=undersampled Fourier encoding matrix with coil sensitivity) and sparsity-promoting l1 norm prior on spatial coefficient matrix *U*, subject to the Frobenius norm constraint on the dictionary *V*. The BCS model simultaneously estimates the sparse spatial coefficients *U* and the dictionary basis functions *V* from the undersampled k-space measurement *b*. To demonstrate the ability of the BCS algorithm, the computer model was implemented to mimic the APT experiment. The simulated phantom contains 9 compartments with different APT-pool concentrations, exchange rates, and semi-solid MT concentrations (water: w, APT: s, MT: m, B_0/B_1=3T/2μT, T_{sat}=5s, T_{1w}/T_{2w}=1.4/0.1s, T_{1s}/T_{2s}=1.4/0.05s, T_{1m}/T_{2m}=1.4s/20μs). For the in-vivo study, all healthy volunteers (N=2) and patients (N=5) were scanned on a Philips 3 T MRI scanner after informed consent was obtained in accordance with the IRB requirement. A fully sampled 2D CEST saturated images were acquired using a TSE sequence with an RF saturation time of 800ms, RF saturation frequency offsets (14 to -8 ppm at intervals of 0.5 ppm), and varied RF saturation power levels (0.5, 1, 1.5, 2 μT for healthy volunteers and 2 μT for tumor patients). The dynamic CEST data was retrospectively undersampled by the golden-angle ordering pattern along RF saturation frequency direction at acceleration R=2, 4, 10, 20, and 50. Water saturation shift-referencing (WASSR) data (26 frequency offsets

from 1.2 to -1.2 ppm at intervals of 0.125 ppm and a saturation power of 0.5μT) was acquired for B_0 corrections (12). As previously used in (2), APT-weighted (APTw) images were quantified by MTR_{asym}(3.5ppm).

Results

Fig. 2 showed the BCS reconstructed APT images of the simulated phantom and the Z-spectrum comparison to the Nyquist sampled, low-resolution acquisition scheme. Accurate APT imaging was successfully achieved using the BCS reconstruction with acceleration factors up to 10. Fig. 3a compared brain APTw images of a typical healthy volunteer (with four different RF saturation powers) under full k-space and BCS acceleration factors of 10. Importantly, accurate BCS reconstructed APTw images without compromising image quality were achieved. The correlation and Bland-Altman analysis were performed to assess the bias and limit of agreement between the full k-space and BCS reconstructed APTw images (Fig. 3b). The BCS reconstructed APTw image had a high correlation with the full k-space reference image (r^2=0.95 for R=10), and the Bland-Altman analysis showed that the bias was significantly small (mean difference of 0.0019% and absolute values for the limits of agreement (±1.96 SD) of +0.69% ~ -0.72%). In the tumor patient study, the Gd-enhancing area (tumor core) on the T_1-weighted post-Gd image was hyperintense on the APTw image (Fig. 4). Again, the accurate APTw image was successfully reconstructed using the BCS algorithm with acceleration factors of up to 10-fold. The mean difference of APTw signals between the full k-space reference and BCS reconstructed images was only 0.15% and 0.09% for the normal (normal appearing white matter) and tumor region (Gd-enhanced tumor core), respectively.

Discussion and Conclusions

We have proposed and valuated a novel BCS-based, dynamic CEST MRI technique for clinical applications. Simulation and in-vivo experiments demonstrated the feasibility of such ultrafast CEST imaging with an acceleration factor up to 10. BCS-based APT imaging acquisition can significantly reduce the scan time and potentially has a wide range of clinical applications, particularly for pediatric patients.

Acknowledgements

No acknowledgement found.

References

(1) Ward KM, Aletras AH, Balaban RS. A new class of contrast agents for MRI based on proton chemical exchange dependent saturation transfer (CEST). J Magn Reson 2000;143:79-87.

(2) Zhou J, Payen J, Wilson DA, Traystman RJ, van Zijl PCM. Using the amide proton signals of intracellular proteins and peptides to detect pH effects in MRI. Nature Med 2003;9:1085-1090.

(3) Ling W, Regatte RR, Navon G, Jerschow A. Assessment of glycosaminoglycan concentration in vivo by chemical exchange-dependent saturation transfer (gagCEST). Proc Natl Acad Sci (USA) 2008;105:2266-2270.

(4) Cai KJ, Haris M, Singh A, Kogan F, Greenberg JH, Hariharan H, Detre JA, Reddy R. Magnetic resonance imaging of glutamate. Nature Med 2012;18:302-306.

(5) Jia G, Abaza R, Williams JD, Zynger DL, Zhou JY, Shah ZK, Patel M, Sammet S, Wei L, Bahnson RR, Knopp MV. Amide proton transfer MR imaging of prostate cancer: A preliminary study. J Magn Reson Imaging 2011;33:647-654.

(6) Dula AN, Asche EM, Landman BA, Welch EB, Pawate S, Sriram S, Gore JC, Smith SA. Development of chemical exchange saturation transfer at 7T. Magn Reson Med 2011;66:831-838.

(7) Togao O, Yoshiura T, Keupp J, Hiwatashi A, Yamashita K, Kikuchi K, Suzuki Y, Suzuki SO, Iwaki T, Hata N, Mizoguchi M, Yoshimoto K, Sagiyama K, Takahashi M, Honda H. Amide proton transfer imaging of adult diffuse gliomas: correlation with histopathological grades. Neuro Oncol 2014;16:441-448.

(8) Tietze A, Blicher J, Mikkelsen IK, Ostergaard L, Strother MK, Smith SA, Donahue MJ. Assessment of ischemic penumbra in patients with hyperacute stroke using amide proton transfer (APT) chemical exchange saturation transfer (CEST) MRI. NMR Biomed 2014;27:163-174.

(9) Tee YK, Harston GW, Blockley N, Okell TW, Levman J, Sheerin F, Cellerini M, Jezzard P, Kennedy J, Payne SJ, Chappell MA. Comparing different analysis methods for quantifying the MRI amide proton transfer (APT) effect in hyperacute stroke patients. NMR Biomed 2014;27:1019-1029.

(10) Li C, Peng S, Wang R, Chen H, Su W, Zhao X, Zhou J, Chen M. Chemical exchange saturation transfer MR imaging of Parkinson's disease at 3 Tesla. Eur Radiol 2014;24:2631-2639.

(11) Bhave S, Lingala SG, Johnson CP, Magnotta VA, Jacob M. Accelerated whole-brain multi-parameter mapping using blind compressed sensing. Magn Reson Med 2015.

(12) Kim M, Gillen J, Landman BA, Zhou J, van Zijl PC. Water saturation shift referencing (WASSR) for chemical exchange saturation transfer (CEST) experiments. Magn Reson Med 2009;61:1441-1450.

Figures

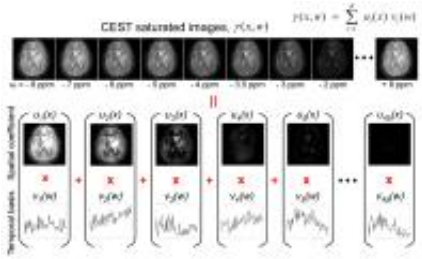

BCS model representation. CEST saturated images are decomposed as a linear combination of spatial weights $u_i(x)$ and temporal basis functions in $v_i(w)$. x is the spatial locations (pixels) and w is saturation frequency measurements.

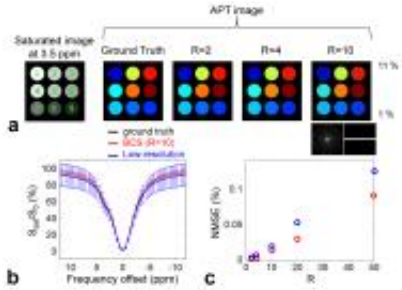

BCS reconstruction of the simulated phantom images. (a) BCS reconstructed APT maps with fully sampled (ground truth) and radial undersampled dataset. (b) corresponding Z-spectrum within the ROI (#3). (c) normalized mean square errors of the BCS and Nyquist sampled linear reconstruction with low-resolution sampling (centeric-ordered).

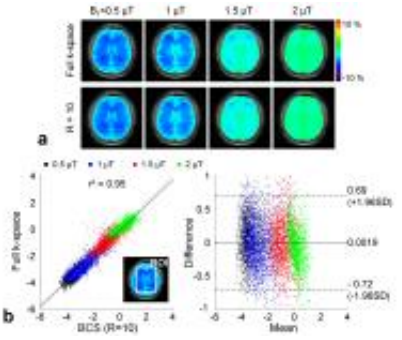

BCS reconstruction of healthy volunteer brain. (a) APTw images with four different RF saturation powers under full k-space and R of 10. (b) correlation plot and Bland-Altman plot to assess the bias and limit of agreement between full k-space and BCS reconstructed APTw images.

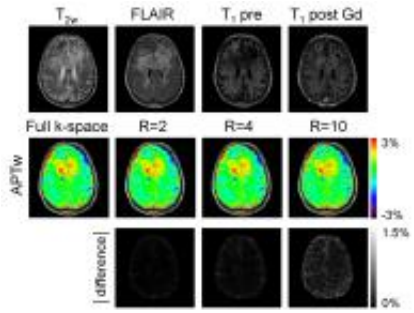

Conventional anatomical images, APTw images, and corresponding difference images with varied BCS acceleration factors for a representative patient with a glioblastoma. The APTw images show clear APTw hyper-intensity in the area of post-Gd enhancement (tumor core).

Proc. Intl. Soc. Mag. Reson. Med. 24 (2016)
0301